



**HAL**  
open science

# Observation of widespread depletion of ozone in the springtime boundary layer of the central Arctic linked to mesoscale synoptic conditions

Hans-Werner Jacobi, Samuel Morin, Jan W. Bottenheim

► **To cite this version:**

Hans-Werner Jacobi, Samuel Morin, Jan W. Bottenheim. Observation of widespread depletion of ozone in the springtime boundary layer of the central Arctic linked to mesoscale synoptic conditions. *Journal of Geophysical Research*, 2010, 115, pp.17302. 10.1029/2010JD013940 . hal-00561265

**HAL Id: hal-00561265**

**<https://hal.science/hal-00561265>**

Submitted on 25 Mar 2021

**HAL** is a multi-disciplinary open access archive for the deposit and dissemination of scientific research documents, whether they are published or not. The documents may come from teaching and research institutions in France or abroad, or from public or private research centers.

L'archive ouverte pluridisciplinaire **HAL**, est destinée au dépôt et à la diffusion de documents scientifiques de niveau recherche, publiés ou non, émanant des établissements d'enseignement et de recherche français ou étrangers, des laboratoires publics ou privés.

# Observation of widespread depletion of ozone in the springtime boundary layer of the central Arctic linked to mesoscale synoptic conditions

Hans-Werner Jacobi,<sup>1,2</sup> Samuel Morin,<sup>3</sup> and Jan W. Bottenheim<sup>4</sup>

Received 25 January 2010; revised 2 April 2010; accepted 14 April 2010; published 3 September 2010.

[1] Recurrent and episodic depletions of ozone (O<sub>3</sub>) in the atmospheric boundary layer have been observed at arctic coastal sites during springtime for the past 25 years. Additional measurements from the central Arctic Ocean in April 2003 and 2007 confirm previous observations in 1994 indicating that low (<5 nmol mol<sup>-1</sup>) O<sub>3</sub> levels most likely represent the normal state of the boundary layer of the Arctic Ocean in springtime. Ozone mixing ratios increase sporadically to typical remote background values only during the approach of lows moving northward into the central Arctic from midlatitudes, bringing O<sub>3</sub>-rich air into the Arctic basin. During a vast majority of the observed O<sub>3</sub> transitions related to the influence of lows, O<sub>3</sub> mixing ratios are strongly negatively correlated to atmospheric pressure. This negative correlation is generally stronger than the correlation between O<sub>3</sub> mixing ratios and air temperature. The observations indicate that the stable boundary layer, which is a large-scale feature of the Arctic Ocean in springtime, may regularly be void of O<sub>3</sub> implying a shift to halogen radicals as the major oxidizing agent on the same spatial scale. The removal of O<sub>3</sub> in the boundary layer on such a large scale may contribute to a reduction of the warming caused by tropospheric O<sub>3</sub> in the Arctic, although the overall impact on the radiation budget is currently unknown.

**Citation:** Jacobi, H.-W., S. Morin, and J. W. Bottenheim (2010), Observation of widespread depletion of ozone in the springtime boundary layer of the central Arctic linked to mesoscale synoptic conditions, *J. Geophys. Res.*, 115, D17302, doi:10.1029/2010JD013940.

## 1. Introduction

[2] In the troposphere, ozone (O<sub>3</sub>) is ubiquitous and acts as an important oxidant and greenhouse gas [Finlayson-Pitts and Pitts, 2000; Intergovernmental Panel on Climate Change (IPCC), 2007]. While the marine atmospheric boundary layer is a net O<sub>3</sub> sink [Wild and Palmer, 2008], its complete removal in the boundary layer is a remarkable phenomenon occurring predominantly in the polar regions, which has been observed in the last 25 years [Bottenheim *et al.*, 1986; Oltmans and Komhyr, 1986; Barrie *et al.*, 1988; Wessel *et al.*, 1998; Simpson *et al.*, 2007]. Such depletion of O<sub>3</sub> is caused by reactive halogen chemistry and occurs regularly in the atmospheric boundary layer during springtime in both polar regions [Simpson *et al.*, 2007].

Termed ozone depletion events (ODEs) because of its sporadic albeit recurring nature at coastal sites [Bottenheim *et al.*, 1986; Simpson *et al.*, 2007; Helmig *et al.*, 2007a], many features of this phenomenon remain poorly determined, including spatial and temporal extent and processes that start or end the ODEs. Previous measurements have already indicated that low O<sub>3</sub> mixing ratios occurred with a higher frequency in the sea ice region compared to coastal locations [Hopper *et al.*, 1994, 1998; Ridley *et al.*, 2003; Bottenheim *et al.*, 2009]. Although Hopper *et al.* [1994] suggested that O<sub>3</sub> mixing ratios over the sea ice were related to the large-scale meteorological condition, they found no significant correlation between O<sub>3</sub> and meteorological data. Here, we analyze additional records of O<sub>3</sub> mixing ratios obtained in springtime over the ice-covered central Arctic between Spitsbergen and the North Pole suggesting that the absence of O<sub>3</sub> in the boundary layer represents the normal state for large areas of the central Arctic at this time of the year. Further analysis reveals that the fast fluctuations in the O<sub>3</sub> mixing ratios are regularly accompanied by opposite changes in atmospheric pressure. We suggest a link between sea ice, the stability, and the chemical composition of the boundary layer over the Arctic Ocean in springtime. Such a link may induce a specific feedback mechanism between atmospheric chemistry and climate in the Arctic. Implications of the absence of O<sub>3</sub> on

<sup>1</sup>Laboratoire de Glaciologie et Géophysique de l'Environnement, Université Joseph Fourier - Grenoble 1, CNRS, Saint Martin d'Hères, France.

<sup>2</sup>Alfred Wegener Institute for Polar and Marine Research, Bremerhaven, Germany.

<sup>3</sup>Météo-France/CNRS, CNRM/GAME, CEN, Saint Martin d'Hères, France.

<sup>4</sup>Environment Canada, Toronto, Ontario, Canada.

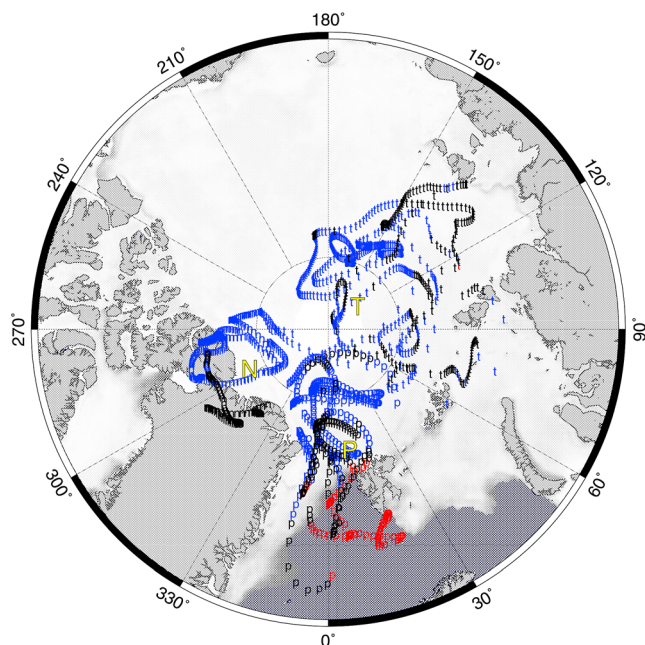


**Figure 1.** Monthly average of the sea ice concentration in April 2003 in the Northern Hemisphere. Yellow capital letters indicate the average positions of *Polarstern* and *TARA* and the location of *Narwhal*. Also shown are the starting points of 24-hr backward trajectories for the measurements during the *Polarstern* (“p”) and *TARA* (“t”) cruises and the ice camp *Narwhal* (“n”) calculated for each full hour of the time series. The colors of the starting points indicate the  $O_3$  mixing ratios measured at the arrival times of the trajectories with less than  $5 \text{ nmol mol}^{-1}$  in blue, more than  $40 \text{ nmol mol}^{-1}$  in red, and values in between in black.

such a large scale for atmospheric oxidation pathways and on the radiative budget of the Arctic are discussed.

## 2. Methods

[3] Ozone measurements were performed onboard of the RV *Polarstern* during the cruise ARK XIX/1 in the first three weeks of April 2003 north of Spitzbergen at the southern edge of the central Arctic [Jacobi et al., 2006; Schauer and Kattner, 2004] and onboard of the schooner *TARA* during a transpolar drift in April 2007 [Bottenheim et al., 2009]. In both cases,  $O_3$  mixing ratios were determined using commercial detectors based on UV absorption. For our analysis we used additional data obtained between 10 and 24 April 1994 during the ice camp *Narwhal* located at the southwestern rim of the central Arctic ( $84^\circ\text{N}$ ,  $63^\circ\text{W}$ ) [Hopper et al., 1998]. Figure 1 shows the mean positions of the ships at  $81.5^\circ\text{N}$  and  $10.2^\circ\text{E}$  for *Polarstern* and at  $87.4^\circ\text{N}$  and  $128.2^\circ\text{W}$  for *TARA* during the selected periods and the location of *Narwhal*.

[4] A full range of meteorological variables is routinely measured onboard of RV *Polarstern*. Information about the different sensors and their installation onboard can be found at [www.awi.de/en/infrastructure/ships/polarstern/meteorological\\_observatory/](http://www.awi.de/en/infrastructure/ships/polarstern/meteorological_observatory/). For the *TARA* cruise and the ice camp *Narwhal*, data from standard meteorological measurements are available as spot values with a time resolution of 1 hr [Hopper

et al., 1998; Vihma et al., 2008]. During the *Polarstern* trip, the synoptic situation summarized in the cruise report [Schauer and Kattner, 2004] was analyzed daily onboard by a meteorologist from the German Weather Service. The reported synoptic conditions agree well with NCEP/NCAR re-analysis data for the northern hemisphere provided by NOAA/OAR/ESRL/PSD, Boulder, Colorado ([www.esrl.noaa.gov/psd/](http://www.esrl.noaa.gov/psd/)) [Kalnay et al., 1996]. To perform a consistent analysis for all three time series, the synoptic conditions were determined using the 6-hourly re-analysis data like the mean sea level pressure, the geopotential heights, and the wind fields.

[5] Starting points of 24-hr backward trajectories for all three  $O_3$  time series were calculated with the Hybrid Single-Particle Lagrangian Integrated Trajectory (HYSPLIT) Model (R. R. Draxler and G. D. Rolph, HYSPLIT (Hybrid Single-Particle Lagrangian Integrated Trajectory) Model, access via [http://www.arl.noaa.gov/HYSPLIT\\_info.php](http://www.arl.noaa.gov/HYSPLIT_info.php)). The model was driven with wind fields with the highest vertical and horizontal resolution available. This is for 1994 the NCEP/NCAR re-analysis data, for 2003 the Final Run re-analysis (FNL) data, and for 2007 the data from the NCEP Global Data Assimilation System (GDAS) model output. Hourly trajectories were calculated for the entire period of the measurements and initiated at the averaged ships’ positions or the position of *Narwhal*. An arrival height of 50 m above the ground level was used for all trajectories. Sea ice concentration was obtained from SSM/I brightness temperatures maps from NSIDC using the ASI algorithm [Kaleschke et al., 2001].

## 3. Results

### 3.1. $O_3$ Levels and Synoptic Conditions

[6] The  $O_3$  time series obtained in April 1994, 2003, and 2007 are shown in Figure 2. All time series exhibit one extended period lasting several days with low  $O_3$  mixing ratios: between 10 and 17 April 1994 with an  $O_3$  maximum of  $3.2 \text{ nmol mol}^{-1}$  (or volumetric part-per-billion, ppbV), 1 and 5 April 2003 with a maximum of  $5.9 \text{ nmol mol}^{-1}$ , and finally 22 and 30 April 2007 with a maximum of  $5.4 \text{ nmol mol}^{-1}$  (Figure 2). During the low  $O_3$  period in 1994, *Narwhal* was located at an edge of a surface high-pressure system [Hopper et al., 1998]. Ozone mixing ratios increased only when the high-pressure system moved out of the region. The synoptic condition in 2003 during the extended period with low  $O_3$  observed onboard the *Polarstern* also remained almost unchanged with a low located southeast of Spitzbergen and an extensive high-pressure system over Northern Greenland (Figure 3). The period after 21 April 2007 on *TARA* was characterized by a persistent high-pressure system around  $80^\circ\text{N}$  and with its center moving between  $100$  and  $170^\circ\text{E}$ . In all three cases persistent and pronounced high-pressure systems caused an air mass flow from the sea ice-covered Arctic Ocean to the sampling area.

[7] In 2003 more than 55% and in 2007 more than 66% of all  $O_3$  observations were below  $5 \text{ nmol mol}^{-1}$  (Figure 4), which is the limit used previously to define ODEs [e.g., Bottenheim et al., 2009]. Less than 20 and 1% in 2003 and 2007, respectively, were larger than  $40 \text{ nmol mol}^{-1}$ . At *Narwhal*, more than 70% of the  $O_3$  observations were below

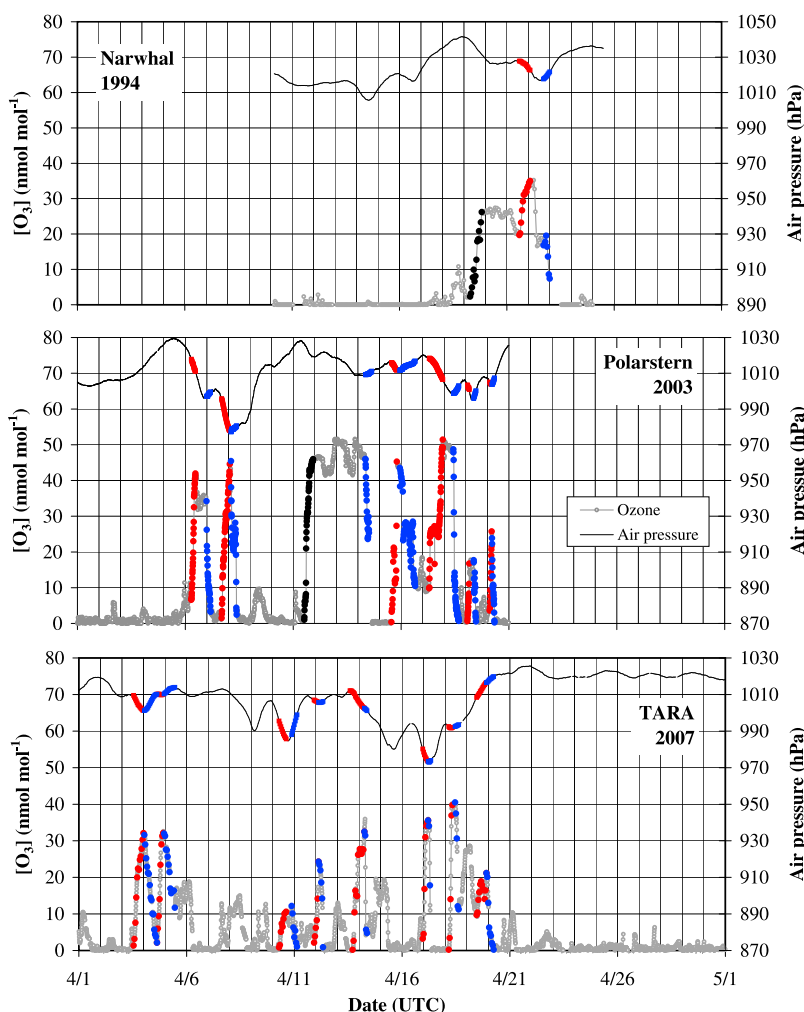


**Figure 2.** Ozone measurements over the Arctic Ocean in April (top) 1994 *Narwhal*, (middle) 2003 *Polarstern*, and (bottom) 2007 *TARA*. The black lines indicate 10-min (*Polarstern*) and 1-hr (*Narwhal*, *TARA*) values of the observed air pressure. Circles indicate 10-min (*Polarstern*, *TARA*) and 1-hr (*Narwhal*) averages of  $O_3$  mixing ratios. Colored symbols indicate  $O_3$  transitions assigned to passing lows (see text) with increasing  $O_3$  in red and decreasing  $O_3$  in blue. The transition periods are also indicated in the air pressure time series. Black symbols indicate ozone increases attributed to the influence of high pressure systems (see text).

$5 \text{ nmol mol}^{-1}$  and all observations remained below  $36 \text{ nmol mol}^{-1}$  (Figure 4). In summary, during all observations low  $O_3$  mixing ratios constituted the prevailing state of the boundary layer and this depleted state was interrupted by episodes with elevated  $O_3$  mixing ratios. The frequency distributions of all three time series (Figure 5) show a weak secondary maximum between 25 and  $30 \text{ nmol mol}^{-1}$  with 3 to 11% of all data points. In the 2003 time series, a third maximum with approximately 10% of all data points appears between 45 and  $50 \text{ nmol mol}^{-1}$ .

### 3.2. Transitions in $O_3$ Levels Related to Meteorological Variables and Synoptic Patterns

[8] The second pronounced feature of the  $O_3$  time series are the fast transitions from low to elevated  $O_3$  and vice versa (Table 1). Often these transitions lasted only a couple of hours with a median of less than 7 hours for all transitions. The detailed analysis of the synoptic conditions using

the mean sea level pressure and the geopotential heights at 850 hPa for all three time series indicate a recurrent pattern of lows influencing the air mass flow at the observational sites for the vast majority of the  $O_3$  transitions. One example of such a passing low is shown in Figure 6 for the observed  $O_3$  transitions from 1.5 to  $44.5$  and back to  $2.4 \text{ nmol mol}^{-1}$  between 7 and 8 April 2003. Starting from low  $O_3$  mixing ratios, the levels increased with the approach of a low from the South bringing air masses from lower latitudes. This airflow continued until the ship was located in the vicinity of the center of the low. Subsequently, the  $O_3$  mixing ratios remained constant and decreased quickly, as soon as the low continued to move farther north leading to an airflow from the Arctic Ocean.

[9] All three time series were analyzed regarding similar relationships between passing lows, changes in air mass transport, and observed  $O_3$  transitions. A total of 31  $O_3$  transitions were identified that we propose to be influenced

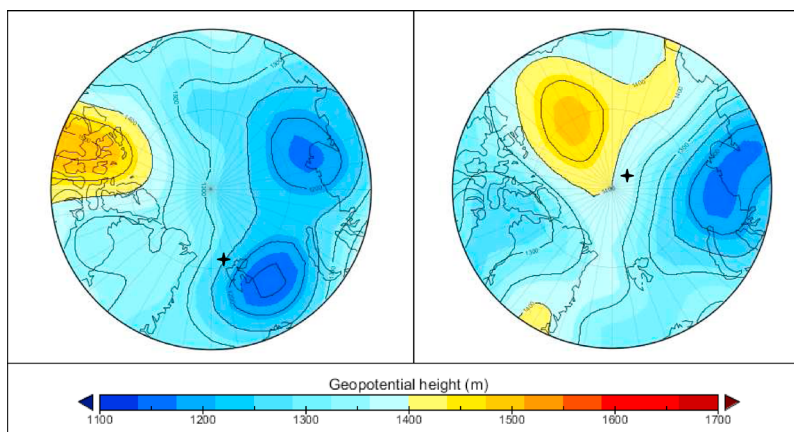


**Figure 3.** Maps of geopotential heights at a level of 850 hPa for (left) 3 April 2003, 12:00 and for (right) 26 April 2007, 12:00 for the area north of 70°N from NCEP/NCAR re-analysis data [Kalnay *et al.*, 1996]. The selected days exemplify conditions typical for the periods with low O<sub>3</sub> mixing ratios measured onboard of *Polarstern* between (left) 1–5 April 2003 and *TARA* (right) 21–30 April 2007. Black stars indicate the location of the ships.

by 16 different lows (*Polarstern* 7, *TARA* 8, and *Narwhal* 1, see Table 1). The identified O<sub>3</sub> transitions are indicated in Figure 2. This concerns most O<sub>3</sub> transitions leading to increases or decreases across a value of 20 nmol mol<sup>-1</sup> (27 out of a total of 32). In all but one cases O<sub>3</sub> peak values of higher than 30 nmol mol<sup>-1</sup> seem to be influenced by the passage of lows. The exception is the increase on 11 April 2003, which is discussed further below. Especially in 2007, further O<sub>3</sub> transitions mainly with peak values remaining below 20 nmol mol<sup>-1</sup> are visible. These transitions are not further analyzed since they were not attributed to any low.

[10] The O<sub>3</sub> transitions attributed to the passage of lows were probed for correlations between the O<sub>3</sub> mixing ratio and meteorological variables like air pressure and temperature. All correlations were restricted to the periods indicated in Table 1. Start and end times of the transitions correspond to the occurrence of minimum and maximum O<sub>3</sub> mixing ratios during the transitions. The differences between minimum and maximum values are also shown in Table 1. From the 31 transitions, a total of four were excluded either due to insufficient data points (two transitions in 2007 with less than five data points) or due to data gaps in the ozone time series (one transition each in 1994 and 2003). The results of the linear regressions between O<sub>3</sub>, pressure, and temperature are summarized in Table 2.

[11] For the remaining transitions, 24 correlations between O<sub>3</sub> and air pressure are statistically significant at the 1% level. All of these transitions show a negative relationship between O<sub>3</sub> and pressure with correlation coefficients ranging from R<sup>2</sup> = 0.40 to 0.98. To test the dependence of the correlations on the selected periods, additional regressions were performed for selected transitions with periods shifted by ±1 hour (N1+, T1+, T2-, T3+, and T4-) or 10 min (P1+, P2-, P3+, and P4-). For most of the examined transitions, the statistical significance of the correlations either remained unchanged or even increased slightly. The overall correlation between O<sub>3</sub> and temperature is less pronounced because only 20 transition show statistically significant correlations. Finally, all 19 transitions with significant correlations between all three variables show the

expected correlations of O<sub>3</sub> mixing ratio, pressure, and temperature.

[12] The O<sub>3</sub> increase on 11 April 2003 (Figure 2), which does not fit into the above described pattern of a passing low, was characterized by a persistent high pressure system between Spitsbergen and Scandinavia (Figure 7). As mentioned by Hopper *et al.* [1998] a similar effect was observed on 19 April 1994 (Figure 2) caused by a surface high-pressure system moving out of the observational region. In both cases, an effective and continuous northward transport of air masses occurred from lower latitudes (in 1994 downward from the Greenland ice sheet [Hopper *et al.*, 1998], in 2003 along the Fram Strait). These are the only two O<sub>3</sub> transitions in the three time series that are related to the influence of high-pressure systems.

### 3.3. Back-Trajectory Analysis

[13] We analyzed backward trajectories for all three time series to examine the relationship between the air masses

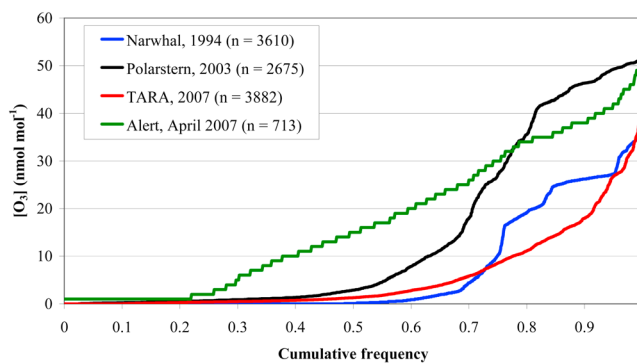


**Figure 4.** Cumulative frequencies of 10-min (*Polarstern*, *TARA*) and 5-min (*Narwhal*) averages of O<sub>3</sub> mixing ratios measured over the Arctic Ocean. Also shown is the cumulative frequency of 1-hr averages of the O<sub>3</sub> mixing ratios measured at Alert in April 2007. The available number of data points is indicated for each location.

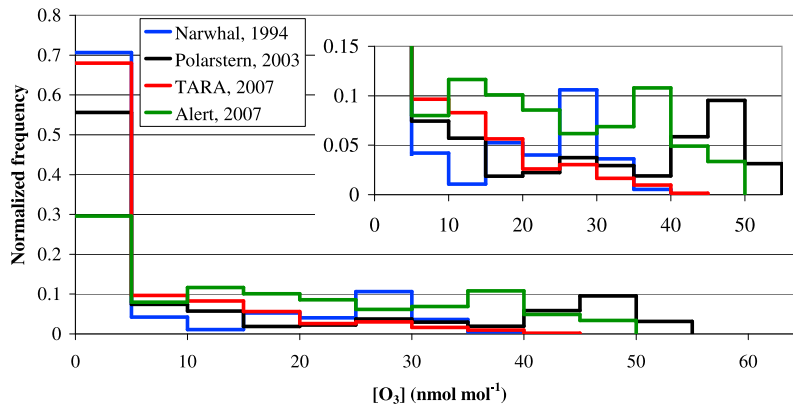


**Figure 5.** Normalized frequency distributions of 10-min (*Polarstern*, *TARA*) and 5-min (*Narwhal*) averages of  $O_3$  mixing ratios measured over the Arctic Ocean. Also shown is the cumulative frequency of 1-hr averages of the  $O_3$  mixing ratios measured at Alert in April 2007. All data points were binned into intervals of  $5 \text{ nmol mol}^{-1} O_3$ .

with high and low  $O_3$  mixing ratios with the previously described influence of the lows. We present here 24-hr backward trajectories to distinguish between the origin of the different air masses. Backward trajectories were calculated for every full hour during the three measurement

periods ending at the respective field sites. The starting points of all trajectories are shown in Figure 1. The air masses probed in 2003 and 2007 always traveled within the boundary layer since all trajectories remained below 200 (2003) and 250 m (2007) altitude. The results indicate that

**Table 1.** Brief Characterization of Lows With Identified Effects on Ozone Transitions in the Observed Time Series<sup>a</sup>

Low	Synoptic Condition <sup>b</sup>	Transition Number	Start (UTC)	End (UTC)	Duration (h)	$\Delta O_3$ ( $\text{nmol mol}^{-1}$ )	Comment
1	Low (1006) at 75°N, 85°E moving north	N1+	21 Apr 14:00	22 Apr 2:00	12:00	+15.3	$O_3$ -p sign.
1	Low (1015) at 85°N, 50°W moving east	N2-	22 Apr 17:00	>23 Apr 0:00	>07:00		Data gap
1	Low (1000) at 75°N, 20°W moving northeast	P1+	6 Apr 6:40	6 Apr 11:20	04:40	+35.3	$O_3$ -p sign.
1	Low (998) at 82.5°N, 10°E moving east	P2-	6 Apr 23:40	7 Apr 4:10	04:30	-30.9	$O_3$ -p sign.
2	Low (984) at 77.5°N, 7.5°W moving northeast	P3+	7 Apr 16:30	8 Apr 1:30	09:00	+43.1	$O_3$ -p sign.
2	Low (976) at 80°N, 0°W moving northeast	P4-	8 Apr 2:50	8 Apr 9:10	06:20	-43.0	$O_3$ -p sign.
3	Low (1005) at 85°N, 5°E moving northeast	P5-	14 Apr 8:20	>14 Apr 22:10	>13:40		Data gap
4	Low (1013) at 82.5°N, 12.5°W moving east	P6+	15 Apr 13:20	15 Apr 19:20	06:00	+44.9	$O_3$ -p sign.
4	Low (1010) at 82.5°N, 10°E moving east	P7-	15 Apr 22:40	16 Apr 15:40	17:00	-33.0	$O_3$ -p sign.
5	Low (1011) at 77.5°N, 20°W moving northeast	P8+	17 Apr 7:20	17 Apr 22:30	15:10	+41.6	$O_3$ -p sign.
5	Low (997) at 82.5°N, 27.5°E moving east	P9-	18 Apr 10:10	18 Apr 16:20	06:10	-48.0	$O_3$ -p sign.
6	Low (993) at 80°N, 40°W moving east	P10+	19 Apr 1:50	19 Apr 3:50	02:00	+16.2	$O_3$ -p sign.
6	Low (994) at 80°N, 10°E dissolving	P11-	19 Apr 8:50	19 Apr 11:20	02:30	-17.2	$O_3$ -p sign.
7	Low (997) at 77.5°N, 7.5°E moving east	P12+	20 Apr 2:40	20 Apr 4:50	02:10	+22.2	$O_3$ -p sign.
7	Low (997) at 77.5°N, 17.5°E moving east	P13-	20 Apr 5:10	20 Apr 8:00	02:50	-23.5	$O_3$ -p sign.
1	Low (987) at 80°N, 100°E moving northwest	T1+	3 Apr 13:00	4 Apr 0:00	11:00	+30.8	$O_3$ -p sign.
1	Low (988) at 82.5°N, 82.5°E moving west	T2-	4 Apr 1:00	4 Apr 15:00	14:00	-29.5	$O_3$ -p sign.
2	Low (988) at 80°N, 60°E moving east	T3+	4 Apr 15:00	4 Apr 22:00	07:00	+30.0	
2	Low (1009) at 80°N, 122.5°E moving west	T4-	4 Apr 23:00	5 Apr 11:00	12:00	-20.3	$O_3$ -p sign.
3	Low (988) at 82.5°N, 87.5°E moving northeast	T5+	10 Apr 7:00	10 Apr 15:00	08:00	+9.8	$O_3$ -p sign.
3	Low (983) at 85°N, 152.5°E moving east	T6-	10 Apr 21:00	11 Apr 3:00	06:00	-11.1	$O_3$ -p sign.
4	Low (991) at 80°N, 7.5°W moving north	T7+	11 Apr 22:00	12 Apr 3:00	05:00	+22.2	$O_3$ -p sign.
4	Low (991) at 82.5°N, 7.5°W moving northwest	T8-	12 Apr 3:00	12 Apr 8:00	05:00	-23.4	$O_3$ -p sign.
5	Low (977) at 77.5°N, 2.5°W moving northeast	T9+	13 Apr 14:00	14 Apr 6:00	16:00	+31.0	$O_3$ -p sign.
5	Low (985) at 85°N, 17.5°E moving northwest	T10-	14 Apr 6:00	14 Apr 9:00	03:00	-27.7	$N < 5$
6	Low (971) at 85°N, 95°E moving north	T11+	16 Apr 23:00	17 Apr 5:00	06:00	+32.4	$O_3$ -p sign.
6	Low (970) at 85°N, 100°E moving north	T12-	17 Apr 5:00	17 Apr 8:00	03:00	-27.7	$N < 5$
7	Low (977) at 80°N, 95°E moving north	T13+	18 Apr 4:00	18 Apr 8:00	04:00	+39.7	
7	Low (977) at 82.5°N, 100°E moving north	T14-	18 Apr 11:00	18 Apr 15:00	04:00	-29.3	$O_3$ -p sign.
8	Low (1000) at 87.5°N, 90°E moving west	T15+	19 Apr 11:00	19 Apr 22:00	11:00	+11.5	
8	Low (1012) at 85°N, 97.5°E dissolving	T16-	19 Apr 22:00	20 Apr 6:00	08:00	-20.0	$O_3$ -p sign.

<sup>a</sup>The lows are numbered for each time series. For low 3 of the *Polarstern* time series only an ozone decrease can be attributed because ozone mixing ratios were already high when the low approached *Polarstern* from the southwest. The ozone transitions are numbered from N1 to N2, P1 to P13, and T1 to T16 at *Narwhal* and for *Polarstern* and *TARA*, respectively. Ozone increases and decreases are marked by + and -. Start and end give the respective times for the ozone transitions, the duration the length of the transitional period. The periods correspond to the red and blue colored points in the ozone time series in Figure 2.  $\Delta O_3$  states the observed changes ozone. The last column indicates if the transitions showed a significant correlation between  $O_3$  and p or if the correlations were omitted due to data gaps or insufficient number of data points (see Table 2).

<sup>b</sup>Pressure in hPa in brackets.

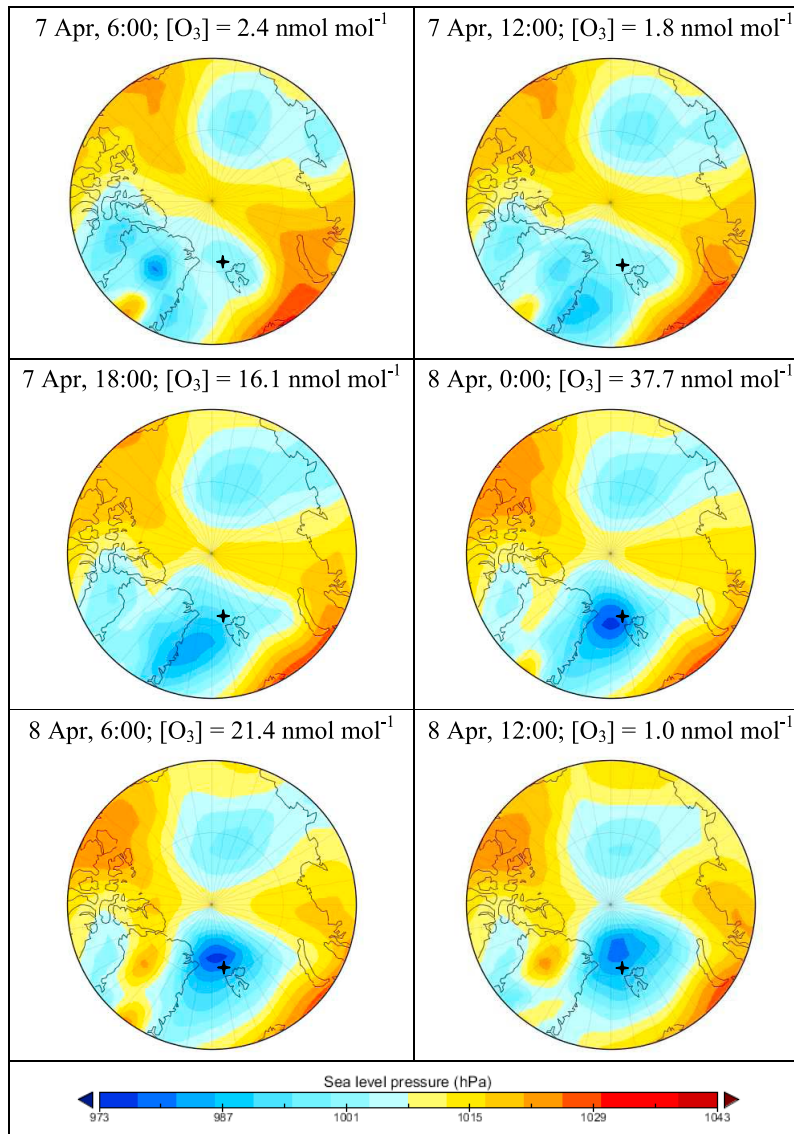


**Figure 6.** Example of a low-passing the location of *Polarstern* (black star, 81.5°N, 10.2°E) between 7 April, 6:00 and 8 April 2003, 12:00. Maps of mean sea level pressure are generated using NCEP/NCAR re-analyses data [Kalnay *et al.*, 1996]. Maps are shown every 6 hours for the region north of 70°N. Observed O<sub>3</sub> mixing ratios are indicated for each map.

in 2003 and 2007 air masses with O<sub>3</sub> mixing ratios higher than 40 nmol mol<sup>-1</sup> almost exclusively were in contact with the marginal ice zone or with open water areas of the North Atlantic within the last 24 hours before reaching the observational sites. In 1994, no 24-hr backward trajectory originated over open water and O<sub>3</sub> values remained below 40 nmol mol<sup>-1</sup>. Air masses with low O<sub>3</sub> mixing ratios (<5 nmol mol<sup>-1</sup>) originated from a much more confined area closer to the field sites and spent always at least 24 hours before arrival over the sea ice region.

#### 4. Discussion

[14] The measurements over the Arctic Ocean reported here are almost opposite to the observations regularly performed at arctic coastal stations [Hopper *et al.*, 1994; Simpson *et al.*, 2007; Helmig *et al.*, 2007a]. To illustrate,

Figure 4 includes also the cumulative frequency of O<sub>3</sub> mixing ratios measured in April 2007 at Alert. Although it is the coastal station in the Arctic encountering most extensive ODEs [Helmig *et al.*, 2007a], Figure 4 demonstrates an almost inverse distribution of O<sub>3</sub> mixing ratios at Alert compared to the Arctic Ocean. A similar difference was reported by Hopper *et al.* [1998] based on the simultaneous O<sub>3</sub> measurements at *Narwhal* and Alert in 1994. Moreover, the frequency distribution for the measurements in April 2007 at Alert shows a secondary maximum between 35 and 40 nmol mol<sup>-1</sup> (Figure 5) in agreement with previous observations by Bottenheim and Chan [2006]. In the time series over the Arctic Ocean this secondary maximum is much less pronounced and shifted to a lower range with O<sub>3</sub> mixing ratios between 25 and 30 nmol mol<sup>-1</sup> (Figure 5). Overall, the conditions over the Arctic Ocean are markedly different compared to the coast. A similar mismatch between

**Table 2.** Results of Linear Regressions Between Ozone Mixing Ratio, Pressure, and Temperature for the Assigned Ozone Transitions of the Three Time Series<sup>a</sup>

Transition Number	[O <sub>3</sub> ] in nmol mol <sup>-1</sup> Versus p in hPa	[O <sub>3</sub> ] in nmol mol <sup>-1</sup> Versus T in °C	T in °C Versus p in hPa
N1+	[O <sub>3</sub> ] = -2.55 · p + 2640; R <sup>2</sup> = 0.73, N = 13	[O <sub>3</sub> ] = 4.92 · T + 120; R <sup>2</sup> = 0.85, N = 13	T = -0.345 · p + 336 R <sup>2</sup> = 0.38, N=13
N2-	Data gap in O <sub>3</sub>	Data gap in O <sub>3</sub>	T = -0.805 · p + 805 R <sup>2</sup> = 0.98
All	[O <sub>3</sub> ] = 0.199 · p + 197; R <sup>2</sup> = 0.03, N = 325	[O <sub>3</sub> ] = 1.34 · T + 44.9; R <sup>2</sup> = 0.57, N = 325	T = 0.285 · p + 320; R <sup>2</sup> = 0.18, N = 357
P1+	[O <sub>3</sub> ] = -6.01 · p + 6120; R <sup>2</sup> = 0.98, N = 29	[O <sub>3</sub> ] = 4.42 · T + 110; R <sup>2</sup> = 0.99, N = 28	T = -1.35 · p + 1340; R <sup>2</sup> = 0.97, N = 28
P2-	[O <sub>3</sub> ] = -6.95 · p + 6950; R <sup>2</sup> = 0.74, N = 27	[O <sub>3</sub> ] = 3.38 · T + 69.1; R <sup>2</sup> = 0.94, N = 27	T = -2.03 · p + 2010; R <sup>2</sup> = 0.69, N = 28
P3+	[O <sub>3</sub> ] = -1.93 · p + 1930; R <sup>2</sup> = 0.96, N = 54	[O <sub>3</sub> ] = 2.39 · T + 53.8; R <sup>2</sup> = 0.97, N = 54	T = -0.797 · p + 774; R <sup>2</sup> = 0.97, N = 55
P4-	[O <sub>3</sub> ] = -7.54 · p + 7400; R <sup>2</sup> = 0.63, N = 39	[O <sub>3</sub> ] = 1.47 · T + 39.4; R <sup>2</sup> = 0.58, N = 39	T = -4.78 · p + 4670; R <sup>2</sup> = 0.95, N = 39
P5-	Data gap in O <sub>3</sub>	Data gap in O <sub>3</sub>	T = -3.71 · p + 3740; R <sup>2</sup> = 0.94, N = 44
P6+	[O <sub>3</sub> ] = -4.68 · p + 4760; R <sup>2</sup> = 0.40, N = 19	[O <sub>3</sub> ] = 5.39 · T + 87.5; R <sup>2</sup> = 0.78, N = 18	T = -0.923 · p + 923; R <sup>2</sup> = 0.66, N = 36
P7-	[O <sub>3</sub> ] = -5.68 · p + 5780; R <sup>2</sup> = 0.82, N = 63	[O <sub>3</sub> ] = 1.55 · T + 50.7; R <sup>2</sup> = 0.01, N = 63	T = -0.0500 · p + 34.2; R <sup>2</sup> = 0.01, N = 103
P8+	[O <sub>3</sub> ] = -1.90 · p + 1960; R <sup>2</sup> = 0.68, N = 69	[O <sub>3</sub> ] = 1.94 · T + 51.7; R <sup>2</sup> = 0.73, N = 69	T = -1.01 · p + 1010; R <sup>2</sup> = 0.99, N = 92
P9-	[O <sub>3</sub> ] = -6.90 · p + 6910; R <sup>2</sup> = 0.46, N = 38	[O <sub>3</sub> ] = 3.36 · T + 49.9; R <sup>2</sup> = 0.68, N = 38	T = -2.41 · p + 2400; R <sup>2</sup> = 0.92, N = 38
P10+	[O <sub>3</sub> ] = -5.05 · p + 5060; R <sup>2</sup> = 0.79, N = 13	[O <sub>3</sub> ] = 6.03 · T + 128; R <sup>2</sup> = 0.91, N = 13	T = -0.860 · p + 842; R <sup>2</sup> = 0.92, N = 13
P11-	[O <sub>3</sub> ] = -3.29 · p + 3290; R <sup>2</sup> = 0.72, N = 16	[O <sub>3</sub> ] = 4.20 · T + 81.0; R <sup>2</sup> = 0.58, N = 16	T = -0.651 · p + 633; R <sup>2</sup> = 0.85, N = 16
P12+	[O <sub>3</sub> ] = -14.5 · p + 14500; R <sup>2</sup> = 0.64, N = 14	[O <sub>3</sub> ] = 7.37 · T + 141; R <sup>2</sup> = 0.68, N = 14	T = -1.63 · p + 1620; R <sup>2</sup> = 0.65, N = 14
P13-	[O <sub>3</sub> ] = -5.01 · p + 5050; R <sup>2</sup> = 0.86, N = 18	[O <sub>3</sub> ] = 4.01 · T + 91.9; R <sup>2</sup> = 0.95, N = 18	T = -1.25 · p + 1230; R <sup>2</sup> = 0.90, N = 18
All	[O <sub>3</sub> ] = 0.0003 · p + 14.3 ; R <sup>2</sup> = 3 · 10 <sup>-8</sup> , N = 2564	[O <sub>3</sub> ] = 1.80 · T + 46.3; R <sup>2</sup> = 0.79, N = 2659	T = -0.0525 · p + 35.2; R <sup>2</sup> = 0.005, N = 2862
T1+	[O <sub>3</sub> ] = -3.70 · p + 3730; R <sup>2</sup> = 0.98, N = 12	[O <sub>3</sub> ] = 2.75 · T + 65.6; R <sup>2</sup> = 0.98, N = 12	T = -1.33 · p + 1320; R <sup>2</sup> = 0.98, N = 12
T2-	[O <sub>3</sub> ] = -2.82 · p + 2850; R <sup>2</sup> = 0.97, N = 15	[O <sub>3</sub> ] = 10.1 · T + 132; R <sup>2</sup> = 0.49, N = 13	T = -0.147 · p + 136; R <sup>2</sup> = 0.55, N = 13
T3+	[O <sub>3</sub> ] = -43.6 · p + 44100; R <sup>2</sup> = 0.44, N = 8	[O <sub>3</sub> ] = 11.6 · T + 172; R <sup>2</sup> = 0.50, N = 8	T = -1.97 · p + 1970; R <sup>2</sup> = 0.24, N = 8
T4-	[O <sub>3</sub> ] = -5.19 · p + 5280; R <sup>2</sup> = 0.94, N = 13	[O <sub>3</sub> ] = -2.74 · T - 15.6; R <sup>2</sup> = 0.10, N = 13	T = 0.135 · p - 151; R <sup>2</sup> = 0.05, N = 13
T5+	[O <sub>3</sub> ] = -1.05 · p + 1040; R <sup>2</sup> = 0.95, N = 9	[O <sub>3</sub> ] = 2.07 · T + 42.2; R <sup>2</sup> = 0.94, N = 9	T = -0.502 · p + 480; R <sup>2</sup> = 0.998, N = 9
T6-	[O <sub>3</sub> ] = -0.978 · p + 978; R <sup>2</sup> = 0.89, N = 7	[O <sub>3</sub> ] = 2.72 · T + 60.1; R <sup>2</sup> = 0.96, N = 7	T = -0.362 · p + 340; R <sup>2</sup> = 0.94, N = 7
T7+	[O <sub>3</sub> ] = -15.9 · p + 16000; R <sup>2</sup> = 0.84, N = 6	[O <sub>3</sub> ] = 3.74 · T + 57.6; R <sup>2</sup> = 0.67, N = 6	T = -3.71 · p + 3720; R <sup>2</sup> = 0.96, N = 6
T8-	[O <sub>3</sub> ] = -34.5 · p + 34700; R <sup>2</sup> = 0.90, N = 6	[O <sub>3</sub> ] = 4.17 · T + 105; R <sup>2</sup> = 0.01, N = 6	T = -0.322 · p + 313; R <sup>2</sup> = 0.13, N = 6
T9+	[O <sub>3</sub> ] = -3.42 · p + 3460; R <sup>2</sup> = 0.92, N = 17	[O <sub>3</sub> ] = 2.06 · T + 38.4; R <sup>2</sup> = 0.92, N = 17	T = -1.60 · p + 1600; R <sup>2</sup> = 0.93, N = 17
T10-	Less than 5 data points		
T11+	[O <sub>3</sub> ] = -5.59 · p + 5480; R <sup>2</sup> = 0.92, N = 7	[O <sub>3</sub> ] = 4.24 · T + 66.0; R <sup>2</sup> = 0.93, N = 7	T = -1.31 · p + 1270; R <sup>2</sup> = 0.98, N = 7
T12-	Less than 5 data points		
T13+	[O <sub>3</sub> ] = -32.0 · p + 31800; R <sup>2</sup> = 0.32, N = 5	[O <sub>3</sub> ] = 5.71 · T + 73.6; R <sup>2</sup> = 0.87, N = 5	T = -7.28 · p + 7210; R <sup>2</sup> = 0.62, N = 5
T14-	[O <sub>3</sub> ] = -33.6 · p + 33400; R <sup>2</sup> = 0.92, N = 5	[O <sub>3</sub> ] = 18.1 · T + 149; R <sup>2</sup> = 0.95, N = 5	T = -1.86 · p + 1840; R <sup>2</sup> = 0.98, N = 5
T15+	[O <sub>3</sub> ] = 0.802 · p + 797; R <sup>2</sup> = 0.45, N = 12	[O <sub>3</sub> ] = -2.37 · T - 10.5; R <sup>2</sup> = 0.26, N = 12	T = -0.246 · p + 238; R <sup>2</sup> = 0.91, N = 12
T16-	[O <sub>3</sub> ] = -6.53 · p + 6650; R <sup>2</sup> = 0.92, N = 9	[O <sub>3</sub> ] = 7.39 · T + 105; R <sup>2</sup> = 0.91, N = 9	T = -0.873 · p + 876; R <sup>2</sup> = 0.98, N = 9
All	[O <sub>3</sub> ] = -0.244 · p + 252 ; R <sup>2</sup> = 0.12, N = 636	[O <sub>3</sub> ] = 0.927 · T + 21.1 ; R <sup>2</sup> = 0.28, N = 699	T = -0.0246 · p + 8.18 ; R <sup>2</sup> = 0.004, N = 700

<sup>a</sup>See Table 1. The numbers correspond to the numbers of the transitions given in Table 1. The linear regressions were performed with ozone mixing ratios in nmol mol<sup>-1</sup>, pressure in hPa, and temperature in °C. “All” indicates the results for linear regression using all data from the time series. For the *Narwhal* data, hourly measurements of the air pressure and temperature and the corresponding 5-min averages of the ozone mixing ratio were used. For the *Polarstern* data, 10-min averages were used. For the *TARA* data, the regressions were performed using the 1-hr spot values of the air pressure and temperature and the corresponding 10-min averages of the ozone mixing ratios. The correlations present the calculated equations of the linear regression lines together with the correlation coefficient R<sup>2</sup> and the number of data points N. Regressions were not performed if less than five data points are available or if data in the O<sub>3</sub> time series are missing. Results for “All” and for linear regressions with a statistical significance of less than 0.01 are printed in italic.

the Arctic Ocean and more southern latitudes were observed during the Tropospheric Ozone Production about the Spring Equinox flights in 2000 [Ridley *et al.*, 2003]. Consequently, statistics based on coastal observations can not be used to infer conditions over the sea-ice covered region. Nevertheless, during specific synoptic situations (e.g. air mass transport from the Arctic Ocean directed to the coast) observations at coastal stations can still deliver information about O<sub>3</sub> mixing ratios over the Arctic Ocean.

[15] The three analyzed springtime time series of O<sub>3</sub> over the Arctic Ocean spanning a period from 1994 to 2007 have several features in common. We assume that these features can be regarded as typical for the boundary layer over the sea ice-covered Arctic Ocean. The driving force for most of the transitions between low and high O<sub>3</sub> seems to be lows that enter the Arctic Ocean from lower latitudes. Persistent highs that lead to similar air mass flows as the described

lows also have the potential to impact the O<sub>3</sub> mixing ratio. It appears that the lows generally induce changes in the transport of air masses originating either from higher or lower latitudes. Consequently, simultaneous changes in meteorological variables as well as O<sub>3</sub> are observed over the Arctic Ocean demonstrated by the apparent (and in most cases significant) correlations between O<sub>3</sub>, pressure, and temperature. However, this implies that these correlations result from a change in air mass flow rather than from pressure- or temperature-dependant processes occurring at or near the field sites and causing the O<sub>3</sub> changes.

[16] The analysis of the backward trajectories indicates that the boundary layer over sea-ice covered areas can be regarded as the origin of air masses with low O<sub>3</sub> levels and low temperatures. This is in agreement with previous observations indicating strong temperature inversions with average surface air temperatures below -20°C in April

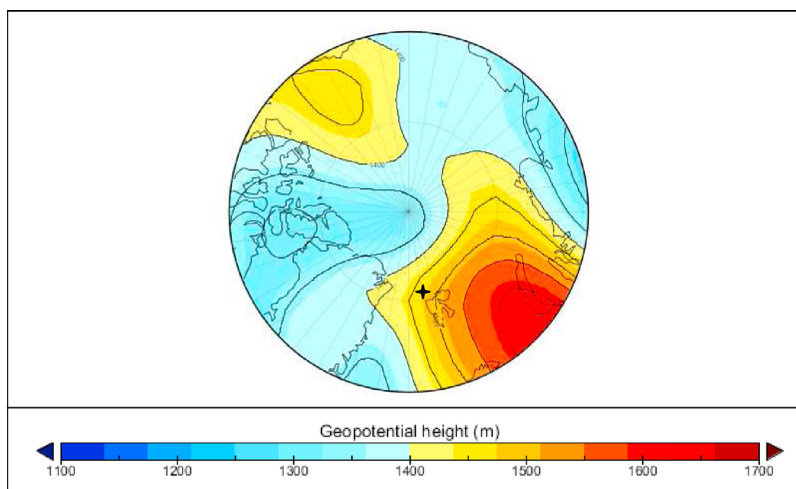


**Figure 7.** Map of geopotential heights at a level of 850 hPa for 12 April 2003, 12:00 for the area north of 70°N from NCEP/NCAR re-analysis data [Kalnay *et al.*, 1996]. The selected day exemplifies conditions typical for the periods with high O<sub>3</sub> mixing ratios between 11–14 April 2003 measured on board of *Polarstern* (black star).

[Kahl *et al.*, 1996] and with a pronounced stability of the boundary layer over the sea ice [e.g., Serreze *et al.*, 1992; Tjernström and Graversen, 2009]. Air masses with low O<sub>3</sub> over the sea ice-covered Arctic Ocean have previously been sampled during several aircraft [Leitch *et al.*, 1994; Jaeschke *et al.*, 1999; Ridley *et al.*, 2003] and ground-based [Morin *et al.*, 2005; Jacobi *et al.*, 2006] measurements. A recent three-dimensional study using a full chemistry-transport model suggested that also the Siberian and Canadian Arctic are characterized by low O<sub>3</sub> mixing ratios [Zhao *et al.*, 2008]. Similarly, a statistical analysis of backward trajectories regarding the origin of air masses with low O<sub>3</sub> mixing ratios in April at three coastal stations in the Arctic (Alert, Barrow, Zeppelin Mountain) also points to large parts of the Arctic Ocean [Bottenheim and Chan, 2006]. Therefore, our conclusion that in the stable boundary layer over sea ice O<sub>3</sub> is absent for longer periods in springtime may be valid for the entire sea-ice covered Arctic Ocean.

[17] The air masses with elevated O<sub>3</sub> can either originate at lower latitudes or at higher altitudes, since background O<sub>3</sub> in springtime are in the range of 40–60 nmol mol<sup>-1</sup> in the polar free troposphere [Anlauf *et al.*, 1994; Hopper *et al.*, 1998; Liang *et al.*, 2009] and 30–50 nmol mol<sup>-1</sup> in the remote boundary layer [Helmig *et al.*, 2007b]. For example, Hopper *et al.* [1998] reported that the increase observed on 20 April 1994 was due to the downward mixing of air from the free troposphere. On the other hand, the 24-hr backward trajectories for 2003 and 2007 indicate that all sampled air masses were transported rather close to the surface. At the same time, mixing ratios above 40 nmol mol<sup>-1</sup> observed in 2003 always originated from open water areas over the North Atlantic characterized by background O<sub>3</sub> mixing ratios. Although we cannot exclude that the O<sub>3</sub> transitions to elevated levels are also influenced by the downward mixing of free tropospheric air masses caused by the approach of the lows, it seems likely that in most cases transport from open water areas at lower latitudes is dominating. A further indication of a preferred horizontal transport may be the

differences in the normalized frequency distributions (Figure 5). The observations performed in 2003 north of Spitzbergen and, thus, relatively close to the open water areas of the eastern half of the Greenland Sea (see Figure 1) exhibit a maximum between 45 and 50 nmol mol<sup>-1</sup>, which is completely absent in the time series from 1994 and 2007, and a further, much weaker maximum between 25 and 30 nmol mol<sup>-1</sup>. In 1994, the maximum between 25 and 30 nmol mol<sup>-1</sup> is much more pronounced. The time series of 2007 also shows a maximum in this range, but again much weaker than in the 1994 time series. This may indicate that longer travel times over the sea ice covered areas may lead to lower peak values of O<sub>3</sub> since the distance of the field sites to the sea ice edge was largest in 2007 and smallest in 2003 (Figure 1).

[18] A sharp transition between low (<5 nmol mol<sup>-1</sup>) and background (>40 nmol mol<sup>-1</sup>) O<sub>3</sub> appears to exist between higher and lower latitudes. The exact position of this transition depends on the mesoscale conditions leading to north- or southward airflow: between the Arctic Ocean and the North Atlantic the average position of the transition correspond roughly to the sea ice edge (Figure 1). This suggests that the chemical composition of the atmospheric boundary layer over the Arctic Ocean is related to a combination of sea ice and mesoscale meteorological conditions. Therefore, a successful modeling of the specific atmospheric composition of the troposphere in this region will require the ability to resolve mesoscale and sea ice conditions as well as the bromine activation leading to the chemical destruction mechanism of O<sub>3</sub>. The presence of sea ice has also a direct impact on O<sub>3</sub> chemistry due to changes in the photolysis rates because of the higher albedo of sea ice compared to open water [Voulgarakis *et al.*, 2009].

## 5. Summary and Implications

[19] In summary, as suggested by Hopper *et al.* [1998] low O<sub>3</sub> mixing ratios of less than 5 nmol mol<sup>-1</sup> are observed over the Arctic Ocean in the presence of sea ice,

sunlight, and probably under stable boundary layer conditions generally associated with low air temperatures. This is in agreement with the results of a modeling study of the development of ODEs using a one-dimensional model [Lehrer *et al.*, 2004]. All three time series with significantly more than half of all data points below  $5 \text{ nmol mol}^{-1} \text{ O}_3$  from very different parts of the Arctic Ocean demonstrate that this is a widespread phenomenon occurring over large parts of the central Arctic Ocean. Nevertheless, this needs to be verified with further ship-based or autonomous monitoring of  $\text{O}_3$  over the Arctic Ocean [Knepp *et al.*, 2010].

### 5.1. Implications for the $\text{O}_3$ Destruction Mechanism

[20] In previous studies, it has been suggested that air temperatures of less than  $-20^\circ\text{C}$  might be a necessary condition for the efficient depletion of  $\text{O}_3$  [Tarasick and Bottenheim, 2002; Bottenheim *et al.*, 2009]. We derived here that the transitions between low and high  $\text{O}_3$  mixing ratios almost always show a strong relationship between  $\text{O}_3$  and air temperature with low  $\text{O}_3$  mixing ratios occurring at low air temperatures. However, the analysis of the meso-scale conditions during these  $\text{O}_3$  transitions indicate that these correlations are the result of transport of air masses with different  $\text{O}_3$  mixing ratios and temperatures. Similar explanations have been reached before [Bottenheim *et al.*, 1990; Morin *et al.*, 2005]. Hence, an observed correlation between  $\text{O}_3$  and temperature can and should not be interpreted as a causal relationship indicating efficient depletion of ozone as a function of lower temperature. In 2003, low  $\text{O}_3$  was observed at air temperatures as high as  $-12^\circ\text{C}$ . The period after 21 April 2007 was characterized by air temperatures above  $-17.5^\circ\text{C}$ , while the  $\text{O}_3$  mixing ratios remained low. Furthermore, Bottenheim *et al.* [2009] reported low  $\text{O}_3$  mixing ratios over the Arctic Ocean in May 2007 even at temperatures as high as  $-6^\circ\text{C}$ . Assuming that these observations indicate ongoing  $\text{O}_3$  depletion would be in contradiction to the hypothesis of Tarasick and Bottenheim [2002]. However, our results imply that these events are simply manifestations of low  $\text{O}_3$  air at higher air temperatures. A similar implication pertains to the assumption that the  $\text{O}_3$  depletion process has to be fast. To the extent that this assumption is a corollary from an observed rapid decrease in the  $\text{O}_3$  mixing ratio our analysis shows that it is not sustainable because the vast majority of the observed transitions can be attributed to a change in air mass flow. A similar conclusion about the lack of conclusive evidence that the chemical  $\text{O}_3$  destruction is a fast process was reached by Bottenheim and Chan [2006].

### 5.2. Implications for the Arctic Climate System

[21] The large-scale removal of  $\text{O}_3$  over the sea ice-covered Arctic Ocean has implications for chemical processes in the atmosphere [Simpson *et al.*, 2007] as well as for the regional radiative budget [IPCC, 2007]. The chemical destruction of  $\text{O}_3$  is closely linked to reaction cycles including reactive halogen compounds [Barrie *et al.*, 1988; Hönninger and Platt, 2002; Simpson *et al.*, 2007] with the oxidative regime shifted to one controlled by halogen reactions. A similar change of the dominating oxidizing agent for nitrogen oxides between April and May in the Arctic was identified using isotope measurements [Morin *et al.*, 2008]. During these months, an enrichment was

reported in the  $^{17}\text{O}$  isotope composition of nitrate in aerosols collected during 16 months at Alert in 2006 and 2007 indicating a substantial contribution of halogens to the oxidation of nitrogen oxides. Such a large imprint in the oxygen isotopes of nitrate seems only possible if the effect of the halogens is not limited to episodes, but rather affects the boundary layer on larger spatial and temporal scales. This contributes further to the growing evidence regarding the impact of reactive halogen species on tropospheric oxidation processes [von Glasow *et al.*, 2004; Read *et al.*, 2008].

[22] Considering a background  $\text{O}_3$  mixing ratio of  $40 \text{ nmol mol}^{-1}$ , the complete removal of  $\text{O}_3$  in a boundary layer with a typical height of approximately 300 m above the surface [Jacobi *et al.*, 2006; Tjernström and Graversen, 2009] as indicated by previous measurements [Roscoe *et al.*, 2001; Ridley *et al.*, 2003; Simpson *et al.*, 2007] corresponds to a reduction of approximately 1.2 Dobson units (DU). Since tropospheric  $\text{O}_3$  acts as a greenhouse gas with a radiative forcing on the order of  $+0.032 \text{ W m}^{-2} \text{ DU}^{-1}$  [IPCC, 2007], this removal corresponds to a negative radiative forcing of approximately  $0.04 \text{ W m}^{-2}$ . As discussed by Simpson *et al.* [2007] the radiative forcing of  $\text{O}_3$  increases with altitude resulting in a smaller forcing by the removal of  $\text{O}_3$  in the boundary layer. Therefore, the full forcing will only develop if the  $\text{O}_3$ -depleted air masses are advected to higher levels. Nevertheless, the removal of  $\text{O}_3$  might counteract a positive forcing that was attributed to an increase in tropospheric  $\text{O}_3$  responsible for an substantial fraction of the observed warming trend between 1890 and 1990 in the Arctic during spring [Shindell *et al.*, 2006]. Finally, reactive halogen compounds can influence the chemistry of dimethyl sulfide emitted by marine sources and, thus, particle formation in marine environments [Carslaw *et al.*, 2010]. Therefore, the removal of  $\text{O}_3$  points to further important direct and indirect links between atmospheric chemistry and the regional climate in the Arctic that warrant further studies.

[23] **Acknowledgments.** We thank the crew of RV *Polarstern* for their assistance and cooperation. The crew of *TARA* and DAMOCLES (European Union 6th Framework Programme 018509) are acknowledged for logistical support and operation of the  $\text{O}_3$  monitor and Hervé Le Goff and Météo France for providing meteorological data. We thank Sunling Gong (Environment Canada) for providing the data from the *Narwhal* 1994 campaign. H.W.J. thanks the German Science Foundation (DFG) for financial support. J.W.B. thanks the Canadian Federal Program Office for the International Polar Year for funding through the IPY project OASIS-Canada (project 2006-SR1-MD-065).

### References

- Anlauf, K. G., R. E. Mickle, and N. B. A. Trivett (1994), Measurement of ozone during Polar Sunrise Experiment 1992, *J. Geophys. Res.*, *99*, 25,345–25,353.
- Barrie, L. A., J. W. Bottenheim, R. C. Schnell, P. J. Crutzen, and R. A. Rasmussen (1988), Ozone destruction and photochemical reactions at polar sunrise in the lower Arctic atmosphere, *Nature*, *334*, 138–141.
- Bottenheim, J. W., and E. Chan (2006), A trajectory study into the origin of spring time Arctic boundary layer ozone depletion, *J. Geophys. Res.*, *111*, D19301, doi:10.1029/2006JD007055.
- Bottenheim, J. W., A. J. Gallant, and K. A. Brice (1986), Measurements of  $\text{NO}_y$  species and  $\text{O}_3$  at  $82^\circ\text{N}$  latitude, *Geophys. Res. Lett.*, *13*, 113–116.
- Bottenheim, J. W., L. A. Barrie, E. Atlas, L. E. Heidt, H. Niki, R. A. Rasmussen, and P. B. Shepson (1990), Depletion of the lower tropospheric ozone during Arctic spring: The Polar Sunrise Experiment 1988, *J. Geophys. Res.*, *95*, 101–127.

- Bottenheim, J. W., S. Netcheva, S. Morin, and S. V. Nghiem (2009), Ozone in the boundary layer air over the Arctic Ocean: Measurements during the TARA transpolar drift 2006–2008, *Atmos. Chem. Phys.*, *9*, 4545–4557.
- Carslaw, K. S., O. Boucher, D. V. Spracklen, G. W. Mann, J. G. L. Rae, S. Woodward, and M. Kulmala (2010), A review of natural aerosol interactions and feedbacks within the Earth system, *Atmos. Chem. Phys.*, *10*, 1701–1737.
- Finlayson-Pitts, B. J., and J. N. Pitts (2000), *Chemistry of the Upper and Lower Atmosphere: Theory, Experiments and Applications*, Academic, San Diego, Calif.
- Helmig, D., S. J. Oltmans, D. Carlson, J. F. Lamarque, A. Jones, C. Labuschagne, K. Anlauf, and K. Hayden (2007a), A review of surface ozone in polar regions, *Atmos. Environ.*, *41*, 5138–5161, doi:10.1016/j.atmosenv.2006.09.053.
- Helmig, D., S. J. Oltmans, T. O. Morse, and J. E. Dibb (2007b), What is causing high ozone at Summit, Greenland?, *Atmos. Environ.*, *41*, 5031–5043, doi:10.1016/j.atmosenv.2006.05.084.
- Hönninger, G., and U. Platt (2002), Observations of BrO and its vertical distribution during surface ozone depletion at Alert, *Atmos. Environ.*, *36*, 2481–2489.
- Hopper, J. F., B. Peters, Y. Yokouchi, H. Niki, B. T. Jobson, P. B. Shepson, and K. Muthuramu (1994), Chemical and meteorological observations at ice camp SWAN during Polar Sunrise Experiment 1992, *J. Geophys. Res.*, *99*, 25,489–25,498.
- Hopper, J. F., L. A. Barrie, A. Silis, W. Hart, A. J. Gallant, and H. Dryfhout (1998), Ozone and meteorology during the 1994 Polar Sunrise Experiment, *J. Geophys. Res.*, *103*, 1481–1492.
- Intergovernmental Panel on Climate Change (IPCC) (2007), *Climate Change 2007: The Physical Science Basis. Contribution of Working Group I to the Fourth Assessment Report of the Intergovernmental Panel on Climate Change*, edited by S. Solomon et al., Cambridge Univ. Press, Cambridge, U. K.
- Jacobi, H. W., L. Kaleschke, A. Richter, A. Rozanov, and J. P. Burrows (2006), Observation of fast ozone loss in the marginal ice zone of the Arctic Ocean, *J. Geophys. Res.*, *111*, D15309, doi:10.1029/2005JD006715.
- Jaeschke, W., T. Salkowski, J. P. Dierssen, J. V. Trümach, U. Krischke, and A. Günther (1999), Measurements of trace substances in the Arctic troposphere as potential precursors and constituents of Arctic haze, *J. Atmos. Chem.*, *34*, 291–319.
- Kahl, J. D. W., D. A. Martinez, and N. A. Zaitseva (1996), Long-term variability in the low-level inversion layer over the Arctic Ocean, *Int. J. Climatol.*, *16*, 1297–1313.
- Kaleschke, L., C. Lüpkes, T. Vihma, J. Haarpaintner, A. Bochert, J. Hartmann, and G. Heygster (2001), SSM/I sea ice remote sensing for mesoscale ocean-atmosphere interaction analysis, *Can. J. Remote Sens.*, *27*(5), 526–537.
- Kalnay, E., et al. (1996), The NCEP/NCAR 40-year reanalysis project, *Bull. Am. Meteorol. Soc.*, *77*(3), 437–471.
- Knapp, T. N., et al. (2010), Development of an autonomous sea tethered buoy for the study of ocean-atmosphere-sea ice-snow pack interactions: The O-buoy, *Atmos. Meas. Tech.*, *3*, 249–261.
- Leitch, W., L. A. Barrie, J. W. Bottenheim, S. M. Li, P. B. Shepson, K. Muthuramu, and Y. Yokouchi (1994), Airborne observations related to ozone depletion at polar sunrise, *J. Geophys. Res.*, *99*, 25,499–25,517.
- Lehrer, E., G. Hönninger, and U. Platt (2004), A one dimensional model study of the mechanism of halogen liberation and vertical transport in the polar troposphere, *Atmos. Chem. Phys.*, *4*, 2427–2440.
- Liang, Q., A. R. Douglass, B. N. Duncan, R. S. Stolarski, and J. C. Witte (2009), The governing processes and timescales of stratosphere-to-troposphere transport and its contribution to ozone in the Arctic troposphere, *Atmos. Chem. Phys.*, *9*, 3011–3025.
- Morin, S., G. Hönninger, R. M. Staebler, and J. W. Bottenheim (2005), A high time resolution study of boundary layer ozone chemistry and dynamics over the Arctic Ocean near Alert, Nunavut, *Geophys. Res. Lett.*, *32*, L08809, doi:10.1029/2004GL022098.
- Morin, S., J. Savarino, M. M. Frey, N. Yan, S. Bekki, J. W. Bottenheim, and J. M. F. Martins (2008), Tracing the origin and fate of NO<sub>x</sub> in the Arctic atmosphere using stable isotopes in nitrate, *Science*, *322*, 730–732, doi:10.1126/science.1161910.
- Oltmans, S. J., and W. D. Komhyr (1986), Surface ozone distributions and variations from 1973–1984 measurements at the NOAA Geophysical Monitoring for Climate Change baseline observatories, *J. Geophys. Res.*, *91*, 5229–5236.
- Read, K. A., et al. (2008), Extensive halogen-mediated ozone destruction over the tropical Atlantic Ocean, *Nature*, *453*, 1232–1235, doi:10.1038/nature07035.
- Ridley, B. A., et al. (2003), Ozone depletion events observed in the high latitude surface layer during the TOPSE aircraft program, *J. Geophys. Res.*, *108*(D4), 8356, doi:10.1029/2001JD001507.
- Roscoe, H. K., K. Kreher, and U. Frieß (2001), Ozone loss episodes in the free Antarctic troposphere, suggesting a possible climate feedback, *Geophys. Res. Lett.*, *28*, 2911–2914.
- Schauer, U., and G. Kattner (2004), The Expedition ARKTIS XIX/1 a, b and XIX/2 of the Research Vessel Polarstern in 2003, *Rep. Polar Mar. Res.* *481*, 194 pp., Alfred Wegener Inst. for Polar and Mar. Res., Bremerhaven, Germany.
- Serreze, M. C., J. D. Kahl, and R. C. Schnell (1992), Low-level temperature inversions of the Eurasian Arctic and comparisons with Soviet drifting stations data, *J. Clim.*, *5*, 615–629.
- Shindell, D., G. Faluvegi, A. Lacis, J. Hansen, R. Ruedy, and E. Aguilar (2006), Role of tropospheric ozone increases in 20th-century climate change, *J. Geophys. Res.*, *111*, D08302, doi:10.1029/2005JD006348.
- Simpson, W. R., et al. (2007), Halogens and their role in polar boundary-layer ozone depletion, *Atmos. Chem. Phys.*, *7*, 4375–4418.
- Tarasick, D. W., and J. W. Bottenheim (2002), Surface ozone depletion episodes in the Arctic and Antarctic from historical ozonesonde records, *Atmos. Chem. Phys.*, *2*, 197–205.
- Tjernström, M., and R. G. Graversen (2009), The vertical structure of the lower Arctic troposphere analysed from observations and the ERA-40 reanalysis, *Q. J. R. Meteorol. Soc.*, *135*, 431–443, doi:10.1002/qj.380.
- Vihma, T., J. Jaagus, E. Jakobson, and T. Palo (2008), Meteorological conditions in the Arctic Ocean in spring and summer 2007 as recorded on the drifting ice station Tara, *Geophys. Res. Lett.*, *35*, L18706, doi:10.1029/2008GL034681.
- von Glasow, R., R. von Kuhlmann, M. Lawrence, U. Platt, and P. J. Crutzen (2004), Impact of reactive bromine chemistry in the troposphere, *Atmos. Chem. Phys.*, *4*, 2481–2497.
- Voulgarakis, A., X. Yang, and J. A. Pyle (2009), How different would tropospheric oxidation be over an ice-free Arctic?, *Geophys. Res. Lett.*, *36*, L23807, doi:10.1029/2009GL040541.
- Wessel, S., S. Aoki, P. Winkler, R. Weller, A. Herber, H. Gernandt, and O. Schrems (1998), Tropospheric ozone depletion in polar regions: A comparison of observations in the Arctic and Antarctic, *Tellus, Ser. B*, *50*, 34–50.
- Wild, O., and P. I. Palmer (2008), How sensitive is tropospheric oxidation to anthropogenic emissions?, *Geophys. Res. Lett.*, *35*, L22802, doi:10.1029/2008GL035718.
- Zhao, T. L., S. L. Gong, J. W. Bottenheim, J. C. McConnell, R. Sander, L. Kaleschke, A. Richter, A. Kerkweg, K. Toyota, and L. A. Barrie (2008), A three-dimensional model study on the production of BrO and Arctic boundary layer ozone depletion, *J. Geophys. Res.*, *113*, D24304, doi:10.1029/2008JD010631.

J. W. Bottenheim, Environment Canada, 4905 Dufferin St., Toronto, ON M3H 5T4, Canada.

H.-W. Jacobi, Laboratoire de Glaciologie et Géophysique de l'Environnement, Université Joseph Fourier - Grenoble 1, CNRS, F-38402 Saint Martin d'Hères, France.

S. Morin, Météo-France/CNRS, CNRM/GAME, CEN, Saint Martin d'Hères F-38402, France.